Utilization of All Hydrothermally Synthesized Red, Green, Blue Nanophosphors for Fabrication of Highly Transparent Monochromatic and Full-Color Plasma Display Devices

*Woo-Seuk Song, Ki-Heon Lee, Young Rag Do, and Heesun Yang**

Visible transparency is one of the attributes pursued in the advancement of display devices. Such a transparency can be realized in a plasma display device simply by applying $Y(V,P)O_4$:Eu red-, $Y(V,P)O_4$:Tm blue-, and $LaPO_4$:Ce,Tb green-emitting nanophosphors with a controlled particle size and reasonable luminescence. The nanophosphors of three primary colors are all hydrothermally synthesized and annealed at appropriate conditions. Highly transparent, uniform emissive layers are deposited by screen-printing the nanophosphor pastes. Using respective screen-printed nanophosphor layers of red, blue, and green, monochromatic transparent test panels of plasma display are fabricated and characterized. Ultimately, a white-luminescing full-color transparent panel is successfully demonstrated by line-patterning the individual nanophosphor layers. Furthermore, for an effort to extract more photons and thus improve the brightness of the test panel, polystyrene monolayer-based 2D photonic crystal is introduced as a scattering medium on the outer surface of the panel and its usefulness was proved.

1. Introduction

Realization of a high degree of visible transparency is among the key issues in the fields of next-generation information display. Transparent emissive display can be demonstrated within the framework of currently available flat panel displays (FPDs), such as organic light-emitting diodes (OLEDs), liquid crystal displays (LCDs), plasma display panels (PDPs. For the evolution into a transparent display the PDP may be regarded as advantageous compared to other competing FPDs because the PDP manufacturing is based on a processing simplicity, cost-effectiveness, and large-size scalability.[1]

The visible transparency is not achievable in the conventional PDPs because of the presence of the opaque components including emissive layers and barrier ribs. In particular, the emissive layers with a typical thickness of ≈20–40 μm are formed using micrometer-sized phosphor particles,[2] thus leading to substantial light scattering in the layers and a total opacity. Introduction of thin-film phosphors that are generally deposited by a vacuum or sol-gel process may significantly improve the visible transparency of emissive layers. However, such thin-film phosphors not only possess processing difficulties, such as high-temperature post-annealing to activate the luminescent centers and a limited choice of substrates that are compatible with the high-temperature annealing, but exhibit low external luminescent efficiencies due to a total internal reflection inside the film.[3–5] Formation of a highly transparent emissive layer is also possible through the solution processing with uniformly small-sized, light scattering-free/-less nanophosphors. Some transparent emissive layers, consisting of either multilayered nanophosphors or nanophosphor-embedded polymer composite, have been produced using green $LaPO_4$:Ce,Tb[6,7] and red YVO_4:Eu nanophosphors;[8] however, more practical work on transparent emissive-layer-based device fabrication has rarely been reported.

Representative three primary color phosphors in the present alternating current (ac)-PDPs are $BaMgAl_{10}O_{17}:Eu^{2+}$ for blue, $Zn_2SiO_4:Mn^{2+}$ for green, and $(Y,Gd)BO_3:Eu^{3+}$ for red emissions.[2] However, uniform nanosizing of those phophors is often challenging due to the compositional complexity, lack of appropriate precursor, or sophisticated synthetic route. Instead, $Y(V,P)O_4$ and $LaPO_4$ phases that possess a high chemical and thermal stability can be chosen as host lattices for doping various rare earth ions in PDP application, since they show high excitation efficiencies under vacuum ultraviolet (VUV) irradiation.[9–14] Moreover, doped $Y(V,P)O_4$ and $LaPO_4$ nanophosphors having a homogeneous size distribution and controlled particle shape can be readily prepared via wet synthetic routes such as hydrothermal,[9–11,15] co-precipitation approaches,[16,17] and their derivatives.

Recently, we reported the hydrothermal preparation of green-emitting $LaPO_4$:Ce,Tb nanophosphors and the fabrication of a transparent panel of a plasma display.[1] In that work, the green nanophosphor-based emissive layer that was formed by spin-casting a nanophosphor suspension showed a high degree of visible transparency, however, the brightness of the fabricated

W. Song, K.-H. Lee, Prof. H. Yang
Department of Materials Science and Engineering
Hongik University
72-1 Sangsu-dong, Mapo-gu, Seoul 121-791, Korea
E-mail: hyang@hongik.ac.kr
Prof. Y. R. Do
Department of Chemistry
Kookmin University
77 Jeongneung-ro, Seongbuk-gu, Seoul 136-702, Korea

DOI: 10.1002/adfm.201102545

test panel was only ≈97 cd m^{-2}. This limited brightness value is mainly attributed to a relatively thin thickness of the emissive layer, which is characteristic of the spin-casting process. To increase a layer thickness through the spin-casting, a tedious, multiple coating is unavoidable. However, the layer uniformity would typically get worse as the number of multiple coating increases. In addition to the above drawbacks of spin-casting, more importantly, it is not a suitable deposition technique for the formation of successive red, green, and blue phosphor patterns in the practical PDP fabrication processing.

In this report, three primary color nanophosphors of red $Y(V,P)O_4$:Eu, blue $Y(V,P)O_4$:Tm, green $LaPO_4$:Ce,Tb are synthesized by a facile hydrothermal route. After optimizing these nanophosphors with respect to size and luminescence through controlling annealing and activator concentration, transparent emissive layers are generated by screen-printing respective nanophosphor pastes. First, utilizing red, blue, and green nanophosphor layers deposited on glass substrate as rear plates, monochromatic transparent panels of plasma display are fabricated and further full-color panel with patterned nanophosphor layers is demonstrated. Detailed transmittance and luminance properties of the test panels are described.

2. Results and Discussion

2.1. Size, Crystal Structure, and VUV Luminescent Properties of Red, Blue, Green Nanophosphors

Scanning electron microscopy (SEM) images of as-synthesized versus annealed red, blue, and green nanophosphors are compared in **Figure 1**. Red $Y(V_{0.5}P_{0.5})O_4$:Eu and blue $Y(V_{0.5}P_{0.5})O_4$:Tm nanophosphors exhibited largely the same size and shape for the as-synthesized (Figure 1a,b) and annealed samples (Figure 1d,f), indicating that the type and amount of activator in the host have little effect on particle growth behavior. The size (10–15 nm) of as-synthesized red and blue nanophosphors a little increased to 35–40 nm upon annealing. The annealing condition of 1000 °C for 1 h was chosen for the red and blue

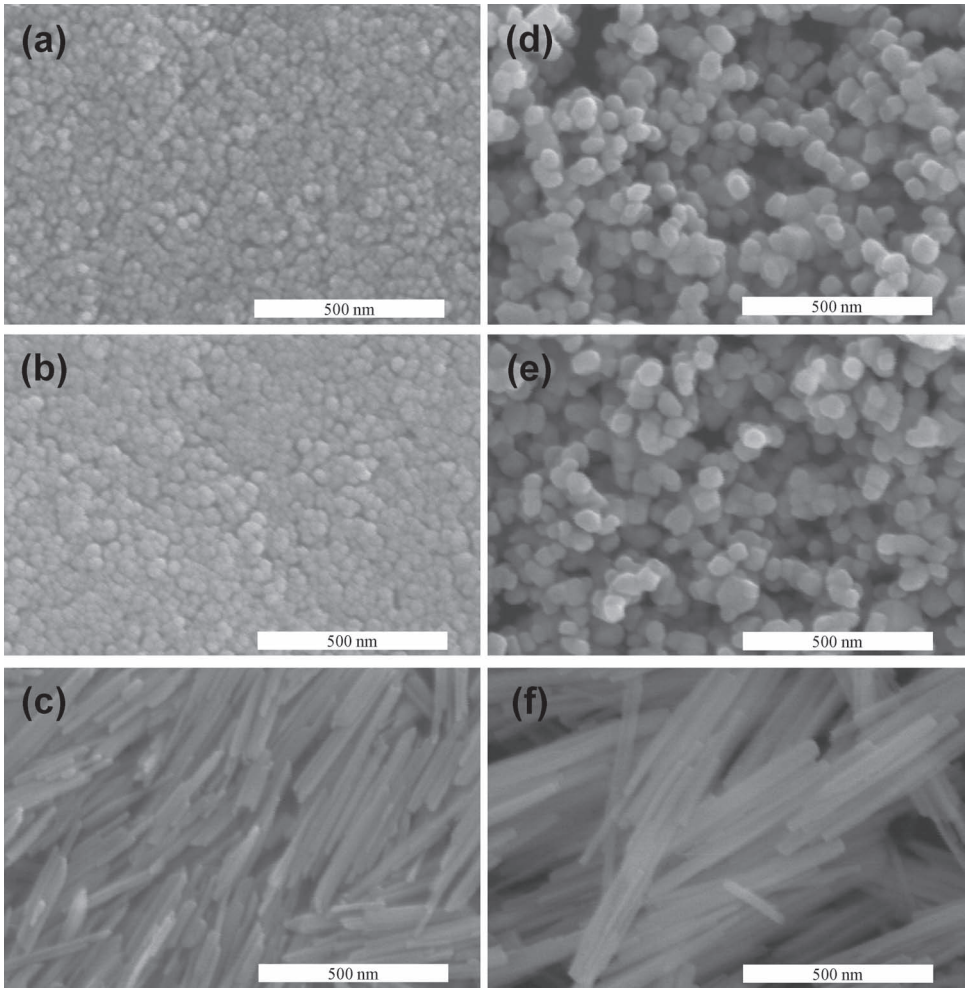

Figure 1. SEM images of as-synthesized a) $Y(V_{0.5}P_{0.5})O_4$:Eu, b) $Y(V_{0.5}P_{0.5})O_4$:Tm, and c) $LaPO_4$:Ce,Tb. 1000 °C-annealed d) $Y(V_{0.5}P_{0.5})O_4$:Eu, e) $Y(V_{0.5}P_{0.5})O_4$:Tm, and f) $LaPO_4$:Ce,Tb nanophosphors. The annealing time was 1 h for $Y(V_{0.5}P_{0.5})O_4$:Eu and $Y(V_{0.5}P_{0.5})O_4$:Tm, and 4 h for $LaPO_4$:Ce,Tb nanophosphors.

nanophosphors. Supplementary annealing tests revealed that either higher annealing temperatures than 1000 °C or longer annealing times than 1 h at 1000 °C led to a substantial particle coarsening and agglomeration, by which the homogeneous distribution in size and shape of nanophosphors could no longer maintained. Green $LaPO_4$:Ce,Tb nanophosphors hydrothermally prepared with the identical condition exhibited 1D morphology with an average diameter of ≈25 nm, as shown in Figure 1c. Hydrothermally synthesized nanocrystalline $LaPO_4$ phase usually showed such an anisotropic morphology due to a preferential growth along *c*-axis,[9,10] although the spherical particles could also be obtainable through the pH control of the starting mixture[16] or the introduction of co-additive.[18] As stated above, Eu- or Tm-doped $Y(V_{0.5}P_{0.5})O_4$ nanophosphors were readily sintered and significantly coarsened upon annealing at 1000 °C for 2 h rather than just 1 h. On the other hand, the size and shape of $LaPO_4$:Ce,Tb nanophosphor were well preserved even after annealing at 1000 °C for a relatively long time of 4 h, even though the average diameter of annealed nanophosphors increased slightly to ≈30 nm (Figure 1f). Based on the melting points of 1995[19] and 1850 °C[20] for xenotime-type YPO_4 and YVO_4, respectively, that of $Y(V_{0.5}P_{0.5})O_4$ phase is expected to lie between the above values. However, monazite-type monoclinic $LaPO_4$ is known to have a higher melting point of around 2072 °C. Therefore, $LaPO_4$:Ce,Tb nanophosphor would be more resistive to the particle coarsening/agglomeration induced during a relatively long time of annealing than $Y(V_{0.5}P_{0.5})O_4$-based nanophosphors.

X-ray diffraction (XRD) patterns of as-synthesized compared to annealed red, blue, and green nanophosphors (the same samples in Figure 1) are shown in **Figure 2**. As expected, the XRD patterns of $Y(V_{0.5}P_{0.5})O_4$:Eu and blue $Y(V_{0.5}P_{0.5})O_4$:Tm nanophosphors were nearly the same for the as-synthesized and annealed samples, consistent with the above SEM results. Extensive peak broadening of the as-synthesized $Y(V_{0.5}P_{0.5})O_4$:Eu or blue $Y(V_{0.5}P_{0.5})O_4$:Tm nanophosphors is attributed to

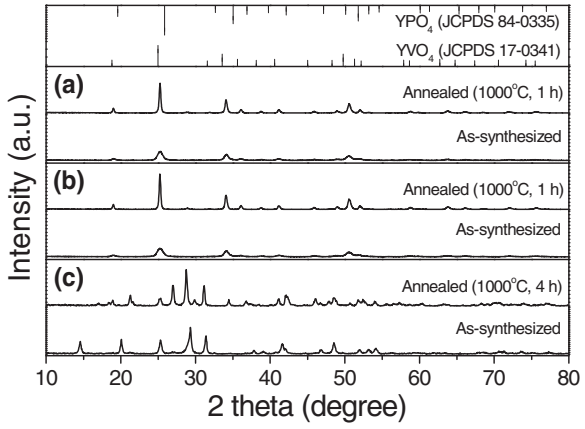

Figure 2. XRD patterns of as-synthesized and annealed a) $Y(V_{0.5}P_{0.5})O_4$:Eu, b) $Y(V_{0.5}P_{0.5})O_4$:Tm, and c) $LaPO_4$:Ce,Tb nanophosphors. The reference patterns of xenotime-type YPO_4 and YVO_4 phases were also included. The patterns of as-synthesized and annealed $LaPO_4$:Ce,Tb nanophosphors well matched with those of hexagonal (JCPDS 75-1881) and monoclinic (JCPDS 32-0496) $LaPO_4$ phase, respectively.

their tiny size, as observed in SEM images (Figure 1a,b). Upon annealing at 1000 °C for 1 h, the full width at half-maximum (FWHM) of the reflection peaks of both nanophosphors became sharper as a result of an improved crystallinity and an increased particle size. Xenotime-type YVO_4 and YPO_4 have the tetragonal zircon structure (space group: $I4_1/amd$) and these isomorphic compounds could be readily intermixed into a homogeneous vanadate/phosphate solid solution.[11–13,21,22] Compared to pure YVO_4 phase, the reflection peaks of our annealed nanophosphors shifted to a higher 2θ. The bond length of P^{5+}–O^{2-} in PO_4^{3-} (1.52 Å) is shorter than that of V^{5+}–O^{2-} in VO_4^{3-} (1.70 Å)[22] due to the smaller radius of P^{5+} (0.34 Å) than that of V^{5+} ion (0.59 Å), and the size of tetrahedral phosphate group is about 8% smaller than that of vanadate group.[13] Therefore, relative to YVO_4 phase, the unit cell of $Y(V_{0.5},P_{0.5})O_4$ would become extracted, resulting in the shift to higher 2θ. For the $LaPO_4$ phase, two polymorphs of low-temperature hexagonal (space group $P6_222$) and high-temperature monoclinic (space group $P2_1/n$) structures exist. In Figure 2c, XRD pattern of as-synthesized $LaPO_4$:Ce,Tb nanophosphor agrees well with that of hexagonal $LaPO_4$ phase (JCPDS 75-1881). However, the crystal structure of the as-synthesized nanophosphor was totally phase-converted to a stable monoclinic monazite-type (JCPDS 32-0496) after 1000 °C annealing. Using Scherrer's equation, the average crystallite sizes of annealed $Y(V_{0.5}P_{0.5})O_4$:Eu (or $Y(V_{0.5}P_{0.5})O_4$:Tm) and $LaPO_4$:Ce,Tb nanophosphors were calculated to be ≈34 and ≈28 nm, respectively, consistent with the above SEM observations.

Vacuum ultraviolet (VUV) photoluminescence (PL) excitation and emission spectra of 1000 °C annealed $Y(V_{0.5}P_{0.5})O_4$:Eu, $Y(V_{0.5}P_{0.5})O_4$:Tm, and $LaPO_4$:Ce,Tb nanophosphors are shown in **Figure 3**a–c, respectively. The excitation bands of $Y(V_{0.5}P_{0.5})O_4$:Eu and $Y(V_{0.5}P_{0.5})O_4$:Tm nanophosphors result from the charge transfer (CT) of R^{3+}–O^{2-} (R = Y, Eu, Tm) and the absorption of PO_4^{3-} and VO_4^{3-}.[12,16,23] In the case of $Y(V_{0.5}P_{0.5})O_4$:Eu, the energy absorbed through the above CT and host absorption processes under VUV excitation is then transferred to VO_4^{3-} and, finally, to the Eu^{3+} center.[12] Characteristic Eu^{3+} red emission peaks result from the multiplet transitions from the excited $^5D_0$ level to the crystal field-split ^7F_J (J = 1, 2, 3, 4) states of Eu^{3+} ion. As seen from Figure 3a, the $^5D_0$–$^7F_2$ transition-related emission line (618 nm) was prevailing over other emission lines at 593 ($^5D_0$–$^7F_1$), 648 ($^5D_0$–$^7F_3$), and 695 nm ($^5D_0$–$^7F_4$) due to the lack of inversion symmetry of $Y(V,P)O_4$ host.[24] It is noted that the VO_4^{3-} group in $Y(V,P)O_4$ host can be a self-emitting luminescent center, showing Stokes-shifted blue wavelengths through the radiative relaxation from the excited to the ground state of VO_4^{3-} group. No appearance of such a blue emission in VUV PL spectrum of $Y(V_{0.5}P_{0.5})O_4$:Eu nanophosphor indicates that the excitation energy of VO_4^{3-} groups was efficiently transferred to the Eu^{3+} center. Upon VUV excitation $Y(V_{0.5}P_{0.5})O_4$:Tm nanophosphor would experience the same gradational energy transfer process as that in $Y(V_{0.5}P_{0.5})O_4$:Eu. Unlike $Y(V_{0.5}P_{0.5})O_4$:Eu nanophosphor, however, the weak VO_4^{3-}–based broad blue emission band around 450 nm was observed along with a dominant Tm^{3+}-related characteristic peak at 475 nm ($^1G_4$–$^3H_6$ transition) and a minor peak at 648 nm ($^1G_4$–$^3H_4$ transition) (Figure 3b).[14,23,25] As shown in Figure 3c, the excitation spectrum of $LaPO_4$:Ce,Tb

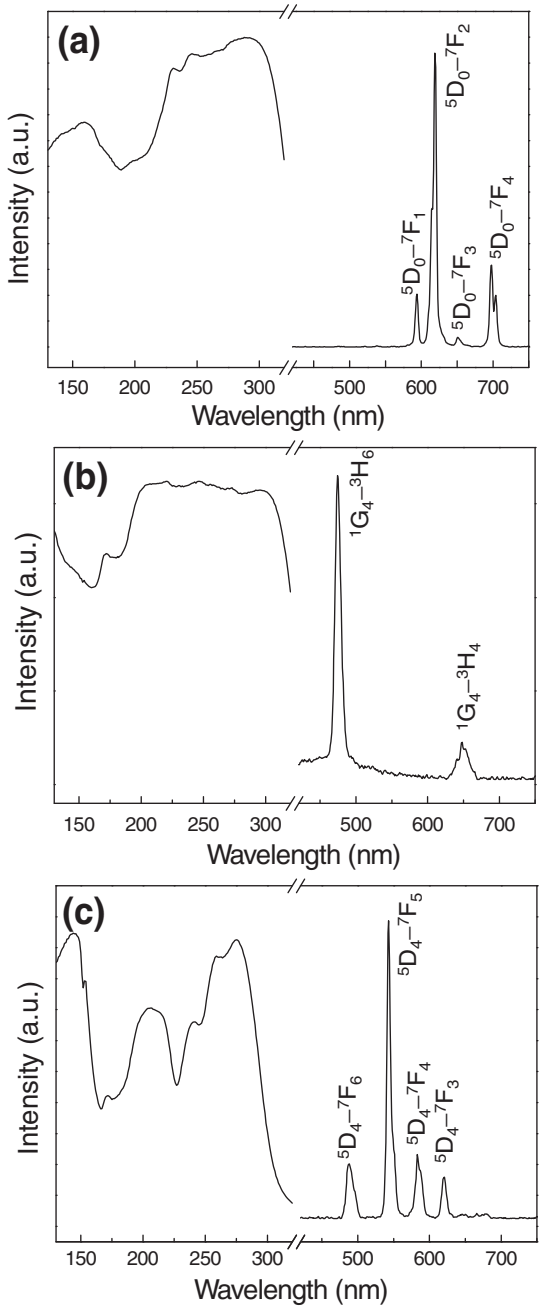

Figure 3. VUV PL excitation and emission spectra of annealed a) $Y(V_{0.5}P_{0.5})O_4$:Eu, b) $Y(V_{0.5}P_{0.5})O_4$:Tm, and c) $LaPO_4$:Ce,Tb nanophosphors. The excitation spectra were recorded with emission wavelengths of 618, 475, and 541 nm for $Y(V_{0.5}P_{0.5})O_4$:Eu, $Y(V_{0.5}P_{0.5})O_4$:Tm, and $LaPO_4$:Ce,Tb nanophosphors, respectively, and all emission spectra were collected with an excitation wavelength of 147 nm.

nanophosphor consists of multiple excitation bands. The first two bands peaking at around 145 nm and 205 nm are ascribed to the absorption of PO_4^{3-} group and the $4f^8 \rightarrow 4f^75d$ transition of Tb^{3+} ion, respectively.[26] The other broad excitation band ranging from 220 to 300 nm can be assigned to Ce^{3+} ion-related transitions between the ground state ($^2F_{5/2}$) and the crystal field-split 5d excited states ($^2D_{5/2}$ and $^2D_{3/2}$).[27,28] The excited Ce^{3+} ion as a donor can efficiently transfer its excitation energy to the excited states of the surrounding Tb^{3+} ion, resulting in an intense Tb^{3+} emission. Tb^{3+}-related characteristic green emission lines in Figure 3c result from f–f transitions of Tb^{3+} ion from $^5D_4$ excited state to ^7F_J (J = 0–6) ground states, showing main emission lines peaking at 488 ($^5D_4$–$^7F_6$), 541 ($^5D_4$–$^7F_5$), 585 ($^5D_4$–$^7F_4$), and 620 nm ($^5D_4$–$^7F_3$). The concentrations of Eu, Tm, and Ce/Tb were varied in order to search the optimal compositions of respective nanophosphors. The x values were 0.03–0.12, 0.001–0.02, and 0.3–0.54 for $Y_{1-x}(V_{0.5}P_{0.5})O_4$:$Eu_x$, $Y_{1-x}(V_{0.5}P_{0.5})O_4$:$Tm_x$, and $La_{0.4}PO_4$:Ce_x,$Tb_{0.6-x}$, respectively, resulting in the highest luminescence efficiencies from the compositions of $Y_{0.94}(V_{0.5}P_{0.5})O_4$:$Eu_{0.06}$, $Y_{0.9975}(V_{0.5}P_{0.5})O_4$:$Tm_{0.0025}$, and $La_{0.4}PO_4$:$Ce_{0.5}$,$Tb_{0.1}$.

2.2. Formation of Red, Green, Blue Emissive Layers and Fabrication of Monochromatic Transparent Panels

The nanophosphor samples of $Y_{0.94}(V_{0.5}P_{0.5})O_4$:$Eu_{0.06}$ and $Y_{0.9975}(V_{0.5}P_{0.5})O_4$:$Tm_{0.0025}$ annealed for 1 h 1000 °C and that of $La_{0.4}PO_4$:$Ce_{0.5}$,$Tb_{0.1}$ annealed for 4 h at 1000 °C were chosen for the following transparent emissive layer formation. After the nanophosphor pastes prepared as described in Experimental Section was ready, each nanophosphor layer was screen-printed on a glass substrate. As shown in **Figure 4**a–c in the photographs of the red, blue, and green nanophosphor layers printed on the glass substrate, all emissive layers exhibit a high degree of visible transparency. As seen in Figure 4d–f, which show the 45°-tilited surface and cross-sectional SEM images of the red, blue, and green nanophosphor layers, respectively, all nanophosphor emissive layers exhibited a similar thickness of 0.9–1.0 μm and a good, uniform layer coverage.

For the quantitative measurement of visible transparency of nanophosphor layer, UV-vis transmittance spectra were collected and are shown in **Figure 5**a. Visible transmittance values (at 550 nm) of the red, blue, and green emissive layers were calculated to be ≈72, ≈74, and ≈73%, respectively, relative to that of the glass substrate (≈91%). These similar transmittance values are consistent with the previous cross-sectional SEM results, which showed almost the same thickness of all nanophosphor layers. Such excellent degrees of visible transparency directly result from an effectively reduced light scattering in the emissive layers. As described in the Experimental Section, the test panel of transparent ac-PDP was fabricated by combining the front and rear plate (nanophosphor/glass). The front plate, which is adopted in the current ac-PDP scheme, has multiple layers of MgO/dielectric layer/BUS + indium tin oxide (ITO) electrodes/glass. Note that the transmittance value of the front plate was about 51% at 550 nm. The transmittance spectra of control (only bare glass as a rear plate) and test panels are compared in Figure 5b. The transmittance value of the control panel without nanophosphor layer was 44% and those of the test panels with red, blue, and green nanophosphors were 33, 35, and 34% at 550 nm, respectively, whose results were naturally consistent with the results of Figure 5a. The see-through capability of the test panel can be seen from the photograph of the representative transparent panel, which has a blue nanophosphor (inset of Figure 5b). There is some room for further

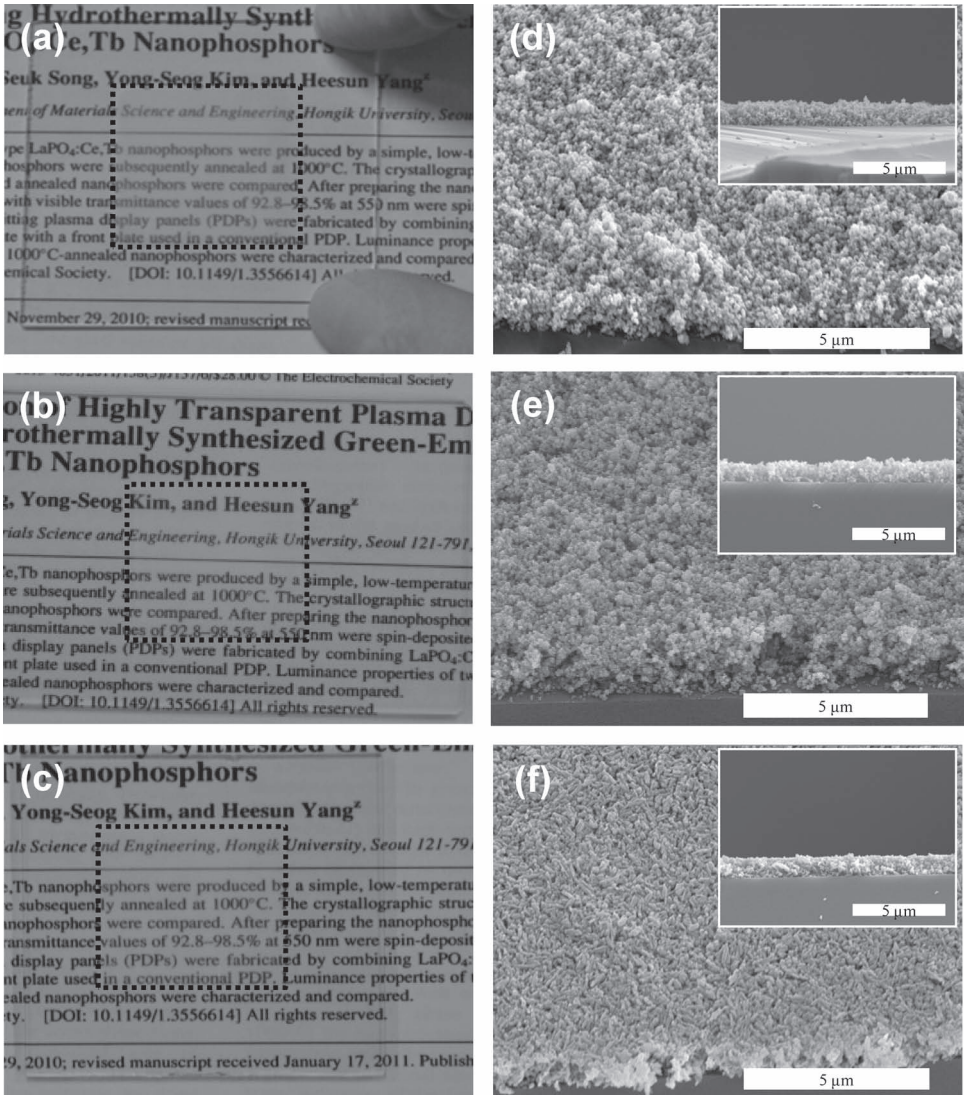

Figure 4. a–c) Photographs and d–f) 45°-tilted SEM surface and cross-sectional (insets) images of screen-printed red, blue, and green emissive, transparent layers on glass substrate. The screen-printed nanophosphor area is marked with a dotted square in (a–c). Panels (a,d), (b,e), and (c,f) correspond to $Y(V_{0.5}P_{0.5})O_4$:Eu, $Y(V_{0.5}P_{0.5})O_4$:Tm, and $LaPO_4$:Ce,Tb nanophosphors, respectively.

enhancing the visible transparency of the panel. For instance, the thickness of dielectric layer of the current front plate is ≈30 μm and its visible transmittance reaches only ≈70%. Thus, a reduction of the dielectric thickness without sacrificing the discharge characteristics of the panel would contribute to a better degree of panel transparency. More conveniently, the thickness of the nanophosphor layer can also be reduced simply by adjusting the amount of nanophosphor powder in the paste, however, a thinner nanophosphor layer with a higher transmittance would result in a reduction in brightness. Therefore, considering a trade-off between transparency and brightness, the thickness of the nanophosphor layer can be compromised.

After loading the test panels into a discharge chamber and filling Ne–Xe gas mixture, 300 V of ac voltage was applied to induce a gas discharge and subsequently generate VUV photons with primary wavelengths of 147 and 172 nm. Upon absorbing these irradiations, each nanophosphor emits a stable, bright luminescence. Normalized discharge luminance spectra of blue-, green-, and red-emitting test panels are shown in **Figure 6**. The insets of Figure 6 present the photographs of the above luminescing panels under gas discharge. The brightness values were measured to be 52, 220, 83 cd m^{-2} from blue-, green-, and red-emitting panels, respectively. White color balancing is one of the important display performance indexes. For white color balancing of the conventional PDP, a typical ratio between red, green, and blue brightness is approximately 28:60:12 in percentage,[29] which is fortunately close to 23:62:15 from our transparent red-, green-, and blue-emitting test panels, respectively.

2.3. Fabrication of a Full-Color Transparent Panel

For the fabrication of full-color transparent test panel, red, green, and blue nanophosphors were consecutively

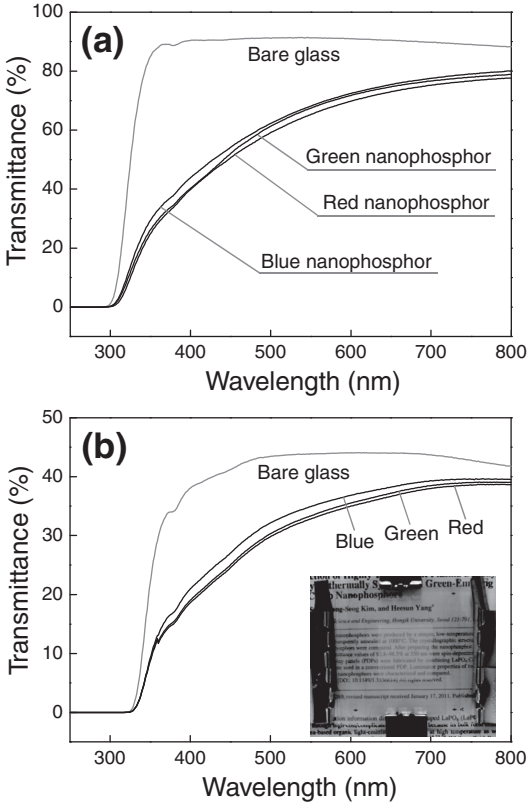

Figure 5. UV-vis transmittance spectra of a) the rear plates and b) the monochromatic test panels with red, blue, and green nanophosphor layers. The rear plate and test panel without the nanophosphor layer (i.e., bare glass only) were also compared. The inset of (b) is a photograph of the representative test panel with a $Y(V_{0.5}P_{0.5})O_4$:Tm blue nanophosphor layer.

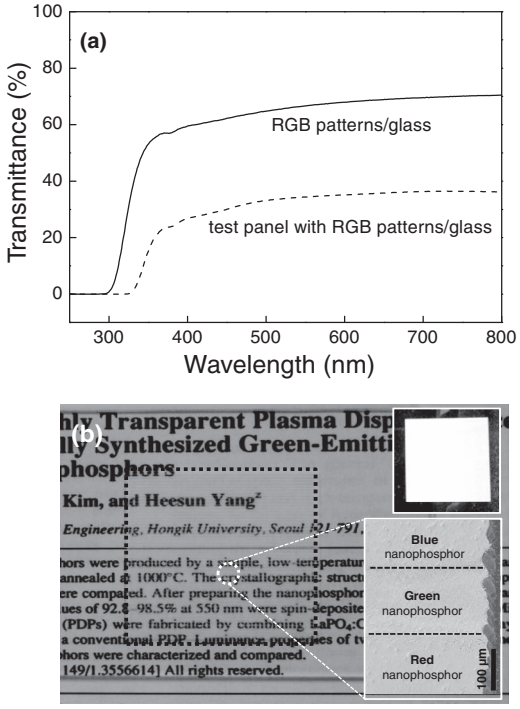

Figure 7. a) UV-vis transmittance spectra of the rear plate and the test panel with line-patterned red, green, blue nanophosphor layers. b) Photograph of line-patterned nanophosphor layers screen-printed on glass. The upper inset is a photograph showing a white emission from nanophosphor patterns under a 254 nm UV irradiation and the lower inset is a low-magnification SEM image of the patterned nanophosphor layers.

screen-printed on glass substrate. UV-vis transmittance spectra of the rear plate (consisting of RGB patterns/glass) and the test panel (combining with the same front plate) are presented in

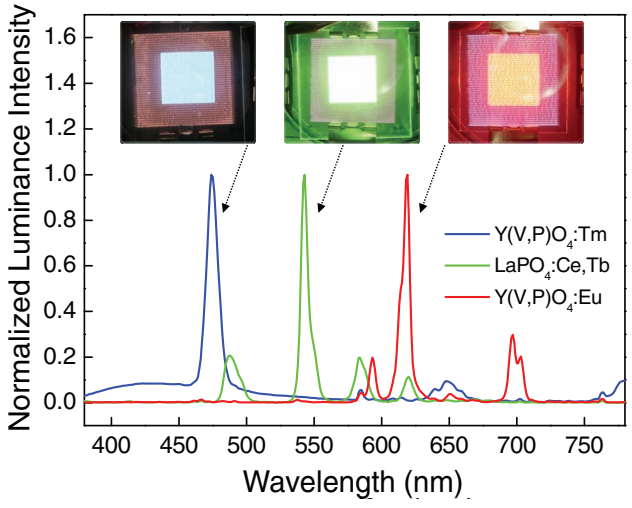

Figure 6. Normalized discharge luminance spectra of three monochromatic test panels with blue, green, and red nanophosphor layers. Photographic images of luminescing panels under gas discharge were also included.

Figure 7a, showing transmittance values (at 550 nm) of 67 and 34%, respectively. These values lie between those of the rear plates with individual red, green, and blue nanophosphors and their monochromatic test panels (Figure 5a,b). The see-through photographic image of the patterned nanophosphors layers/glass is presented in Figure 7b and a white emission from the same sample can also be observed under a 254 nm UV illumination (upper inset of Figure 7b). A low-magnification SEM image of uniformly patterned nanophosphor layers is shown in the lower inset of Figure 7b. The discharge luminance test of the full-color transparent panel was conducted in the same way as in the monochromatic panels. As shown in **Figure 8**a, the white luminance spectrum consists of Tm^{3+}-, Tb^{3+}-, and Eu^{3+}-related characteristic emission peaks from individual nanophosphor layers, resulting in a brightness of 96 cd m^{-2}. The photograph of the white luminescing test panel and the optical microscopy image (inset) of magnified nanophosphor layer patterns are shown in Figure 8b. The Commission International d'Eclairage (CIE) chromaticity coordinates of the white light from the panel were (0.34, 0.37) (as marked with a star in inset of Figure 8a), which is quite close to an ideal white point of (0.33, 0.33).[30,31]

Compared with a standard video brightness of 200 cd m^{-2} for conventional opaque display devices,[32] the brightness of the full-color transparent panel was not high. For our test panel, the photons emitted from the nanophosphors enter

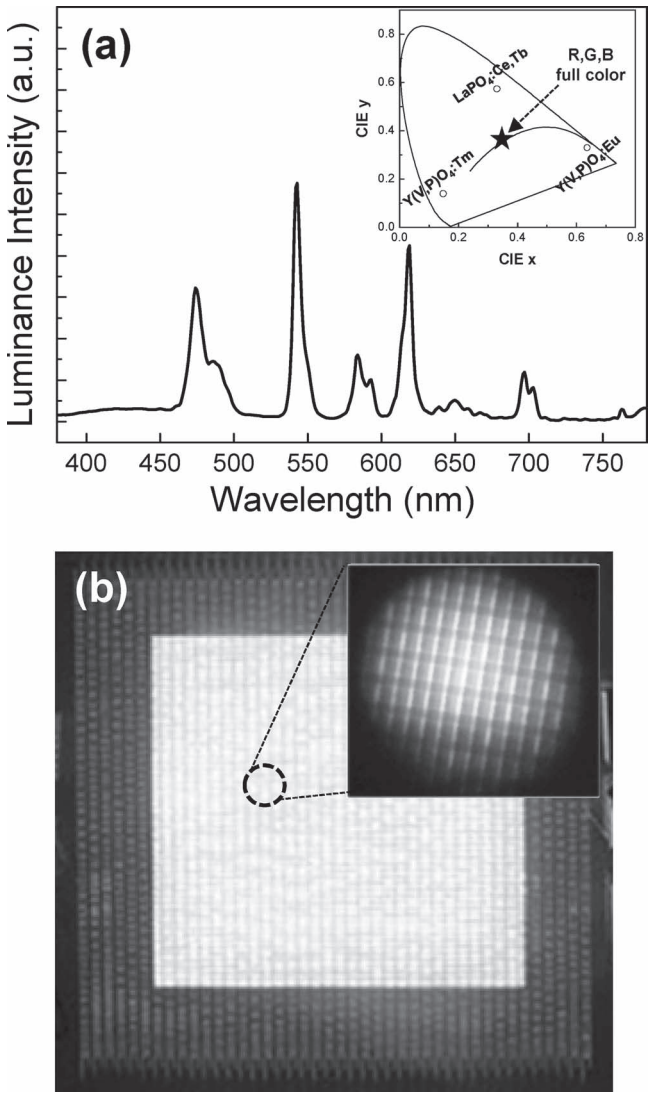

Figure 8. a) Discharge luminance spectrum and b) photograph of a white-luminescing full-color transparent panel under gas discharge. The CIE chromaticity coordinates of the white emission from the panel were marked in the inset of (a). Inset of (b) is a magnified optical microscopy image, showing red, green, and blue nanophosphor layer patterns.

the glass substrate of rear plate and a fraction of photons can escape from the glass. A large portion of photons inside the glass would undergo a waveguide effect due to the total internal reflection at the glass/air interface, originating from the difference in refractive index (n) between glass (1.51) substrate and air (1). The fraction propagating externally among the photons inside the glass can be calculated to be only ≈11% according to the relation of $1/4n^2$.[3,33] Therefore, for an effort to improve the brightness of our full-color test panel, polystyrene (PS) monolayer (ML)-based 2D photonic crystal layer was introduced. 2D photonic crystal has proved to be effective in enhancing light extraction efficiency in the fields of thin-film phosphors[3–5] and OLEDs,[34,35] acting as a leaky and/or Bragg scattering medium for perturbing the waveguided light.

Using monodisperse PS colloids with a diameter of 420 nm, PS ML was formed on the outer surface of the rear plate by a scooping transfer method (see Experimental Section for details). Uniform ML of self-assembled, hexagonally close-packed PS arrays can be seen in **Figure 9**a. Upon PS ML formation, the rear plate exhibited a reduced visible transmittance value along with a transmittance dip due to a 2D photonic crystal stop band, as shown in Figure 9b. Discharge luminance spectra of the full-color panels without versus with PS ML are compared in Figure 9c. The panel covered with PS ML exhibited an enhanced brightness of 137 cd m^{-2}, which is ≈43% increase compared with that of the same panel without PS ML. This improvement in brightness demonstrates that the scattering layer of PS ML was effective in perturbing the waveguided photons inside glass, resulting in an enhanced efficiency of light extraction out of glass. The photograph of a white-luminescing full-color transparent panel (under gas discharge), where only one side of the rear plate was covered with PS ML, is shown in Figure 9d.

3. Conclusions

Choosing the compositions of $Y(V_{0.5},P_{0.5})O_4$:Eu, $Y(V_{0.5},P_{0.5})O_4$:Tm, and $LaPO_4$:Ce,Tb, the identical hydrothermal synthesis was carried out for production of red, blue, and green nanophosphors. As-prepared nanophosphors were then annealed at 1000 °C for different periods of time, depending on the nanophosphor composition. Using the annealed nanophosphors with optimized activator concentrations, nanophosphor-based transparent emissive layers with a thickness of 0.9–1.0 μm were uniformly generated by a screen-printing process. All nanophosphor layers exhibited excellent degrees of visible transparency with higher transmittance values than 70% at 550 nm. Monochromatic test panels of plasma display were fabricated by the simple combination of the rear plate (nanophosphor/glass) with the front plate of the current ac-PDPs and exhibited discharge brightness values of 52, 220, and 83 cd m^{-2} from blue-, green-, and red-emitting panels, respectively. A full-color transparent panel was fabricated by generating line-patterned red, green, and blue nanophosphor layers through a successive screen-printing process. The full-color test panel exhibited a similar visible transmittance to monochromatic panels and a white emission with a brightness of 96 cd m^{-2} and a CIE coordinates of (0.34, 0.37). Additionally, a 2D photonic crystal of PS ML was introduced to the full-color test panel to extract the photons waveguided inside the glass of rear plate. The panel with PS ML showed a brightness of 137 cd m^{-2}, demonstrating that the scattering layer of PS ML was effective in enhancing the panel brightness.

4. Experimental Section

Synthesis of Red, Blue, and Green Nanophosphors: Y (III) nitrate ($Y(NO_3)_3{\cdot}6H_2O$, 99.8%), sodium orthovanadate (Na_3VO_4, 99.98%), sodium phosphate (Na_3PO_4, 96%), Eu (III) nitrate ($Eu(NO_3)_3{\cdot}5H_2O$, 99.9%), Tm (III) nitrate ($Tm(NO_3)_3{\cdot}5H_2O$, 99.9%), La (III) nitrate ($La(NO_3)_3{\cdot}6H_2O$, 99.99%), Ce (III) nitrate ($Ce(NO_3)_3{\cdot}6H_2O$, 99.999%), Tb (III) nitrate ($Tb(NO_3)_3{\cdot}5H_2O$, 99.9%), and phosphoric acid (H_3PO_4, ≥98%) were purchased from Aldrich and used as received.

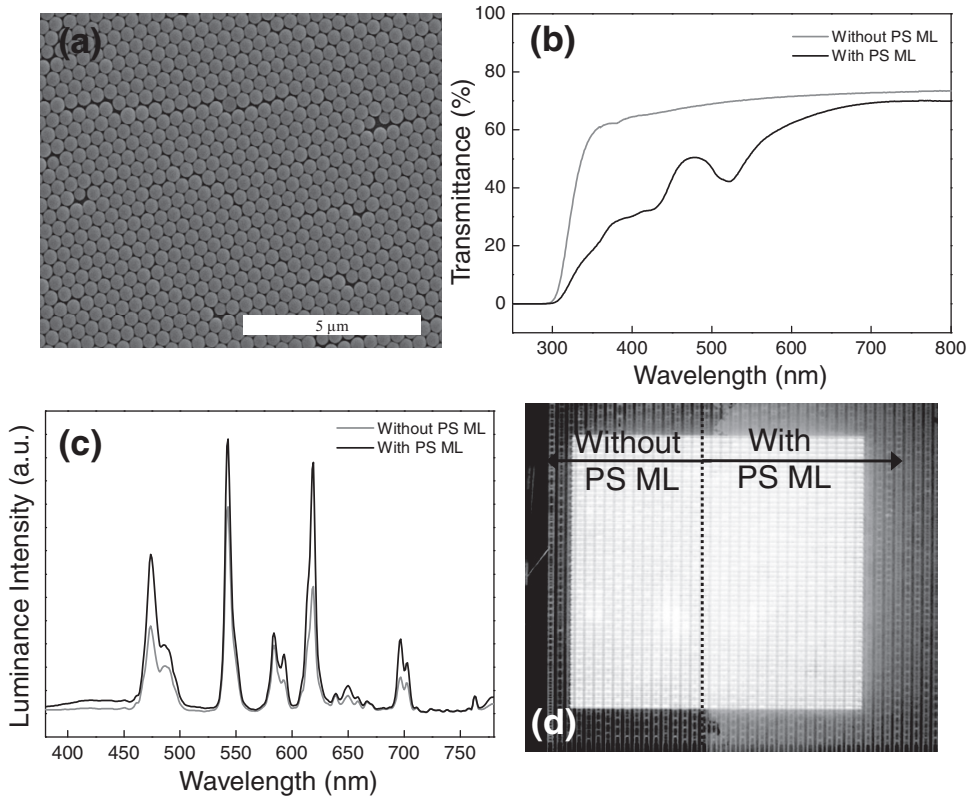

Figure 9. a) SEM image of a hexagonally close-packed PS ML, b) UV-vis transmittance spectra of RGB patterned rear plate without versus with PS ML, c) discharge luminance spectra of the full-color test panel plate without versus with PS ML, and d) photograph of a white-luminescing full-color transparent panel with only one side of the rear plate covered with PS ML under gas discharge.

For a typical preparation of red-emitting $Y_{0.94}(V_{0.5},P_{0.5})O_4:Eu_{0.06}$ nanophosphor, stoichiometric amounts of Y nitrate (9.4 mmol) and Eu nitrate (0.6 mmol) were dissolved in 30 mL of DI water, followed by the addition of sodium orthovanadate (5 mmol) and sodium phosphate (5 mmol) to the above transparent aqueous solution. And then the above mixture was loaded into a 50 mL Teflon-lined stainless steel autoclave and sealed. The autoclave was placed in the oven preheated at 170 °C and maintained at that temperature for 2 h for hydrothermal reaction. The Eu concentration was also varied within $x = 0.03$ to 0.12 in $Y_{1-x}(V_{0.5},P_{0.5})O_4:Eu_x$. Hydrothermal synthesis of blue-emitting $Y_{1-x}(V_{0.5},P_{0.5})O_4:Tm_x$ nanophosphors was exactly the same as that of $Y(V_{0.5},P_{0.5})O_4$:Eu except for use of Tm nitrate with $x = 0.001$–0.02. In a typical synthesis of green-emitting $La_{0.4}PO_4:Ce_{0.5},Tb_{0.1}$ nanophosphor, 4 mmol of La nitrate, 5 mmol of Ce nitrate, 1 mmol of Tb nitrate were dissolved in 30 mL of deionized (DI) water and 10 mmol of phosphoric acid was then added to the above solution. And the above hydrothermal procedure and condition were applied identically. The $La_{0.4}PO_4:Ce_{0.6-x},Tb_x$ nanophosphors with different Ce:Tb ratios of $x = 0.06$–0.3 were also synthesized. The resulting red, blue, and green nanophosphors were precipitated and purified repeatedly with acetone by centrifugation. The precipitates were dried at 90 °C for 1 h and subsequently were annealed at 1000 °C for different periods of time in an air atmosphere.

Formation of Transparent Emissive Layers and Fabrication of Monochromatic Transparent Test Panels: First, the nanophosphor pastes suitable for a screen printing were prepared as follows; 0.4 g of each red, blue, and green nanophosphor was dispersed in 15 mL of 2-methoxyethanol with a standard ultrasonicator for 3 to 5 h and 3 mL of a commercial PDP organic vehicle was blended with the above nanophosphor dispersion. 2-methoxyethanol was eliminated by heating the mixture to 120 °C. With the resulting nanophosphor paste, transparent nanophosphor emissive layer with an area of 2.5 × 2.5 cm^2 was screen-printed on 6 × 6 cm^2 sized, 5 mm thick soda lime glass substrate with a rubber squeegee. The as-printed nanophosphor layer was baked at 150 °C for 30 min and subsequently calcined at 470 °C for 40 min to remove the organic vehicle.

A red, blue, or green-emitting monochromatic test panel of transparent ac-PDP was simply demonstrated by combining the above rear plate (nanophosphor layer/glass) with the front plate used in the current ac-PDPs. The front plate consists of two line-patterned ITO/silver BUS discharge electrodes, 30 μm dielectric layer, and 500 nm thick MgO protection layer on glass substrate. The combined test panel was loaded in the discharge chamber, which was subsequently filled with a Ne with 20% Xe gas mixture up to a gas pressure of 400 Torr. For the discharge luminance test, the combined test panel was placed in the discharge chamber and a Ne and 20% Xe gas mixture was filled with a gas pressure of 400 Torr. Through applying an ac voltage of 300 V (frequency of 30 kHz), a gas discharge was initiated and maintained, generating VUV irradiation of the Xe-related resonance line (147 nm) and molecular band (172 nm).

Fabrication of Full-Color Transparent Panel and Formation of PS ML 2D Photonic Crystal: The above-mentioned red, green, and blue nanophosphor pastes were used for the formation of red-green-blue (RGB) emissive layer patterns on glass substrate. Line-patterned nanophosphor layers were generated by a manual screen-printing in the sequence red, then green, then blue. The following details in the fabrication of full-color transparent panel were the same as those of monochromatic test panels. In an effort to enhance the light extraction efficiency of the full-color panel, a 2D photonic crystal of PS ML was formed on the outer surface of the rear plate (RGB patterns/glass) using a scooping transfer technique.[3,36] Starting with monodisperse

PS colloids (420 nm, Interfacial Dynamics Co.), the formation of PS ML consisted of three steps: floating, crystallization, and the transfer processes. First, an aqueous suspension of 4.4 wt% PS colloids was diluted with an equal volume of ethanol. Several drops of the diluted PS suspension were carefully introduced onto the water surface using a UV/ozone-treated, hydrophilic Si wafer. Second, the floating PS colloids on the water surface self-assembled (or crystallized) and grew to into a large domain upon adding a few drops of sodium dodecyl sulfate ($NaC_{12}H_{25}SO_4$, SDS). The addition of SDS was necessary to generate a rigid PS ML domain because it modifies the surface tension of water.[3] Last, the floating large PS ML domain on the water surface was transferred onto the outside surface of the rear plate by immersing and scooping it. Transferred PS ML on the rear plate was dried on a hot plate at 60 °C for 30 min.

Characterization: A field emission SEM (Hitachi S-4300) operated at 10 kV was used to obtain information on the size and shape of nanophosphors and the morphology of the transparent emissive layers. Phase identification of as-synthesized and annealed red, blue, and green nanophosphors was carried out by XRD using a Rigaku Ultima IV diffractometer with Cu K_α radiation source. VUV PL emission spectra of the nanophosphor powders were collected with an excitation wavelength of 147 nm using a D_2 lamp and a charge-coupled device detector (PTE-VUVD2L2000, PSI). VUV PL excitation spectra were also recorded with a photomultiplier tube detector and corrected with the signal of sodium salicylate powder (reference material). UV-vis transmittance characteristics of the rear plates (nanophosphor layer/glass) and combined test panels were measured with a mode of normal incidence to substrate surface using UV-vis spectroscopy (Shimadzu, UV-2450). Discharge luminance properties of the monochromatic and full-color transparent panels were measured using a spectroradiometer (CS-1000, Minolta).

Acknowledgements

This research was supported by a grant (F0004071-2011-33) from the Information Display R&D Center, one of the Knowledge Economy Frontier R&D Programs funded by the Ministry of Knowledge Economy of Korean government.

Received: October 22, 2011
Published online: February 10, 2012

[1] H. Zhu, G. Ou, L. Gao, *Mater. Chem. Phys.* **2010**, *121*, 414.
[2] H. Zhu, E. Zhu, H. Yang, L. Wang, D. Jin, K. Yao, *J. Am. Ceram. Soc.* **2008**, *91*, 1682.
[3] X. Hu, S. Yan, L. Ma, G. Wan, J. Hu, *Powder Technol.* **2009**, *192*, 27.
[4] P. Yang, Z. Quan, C. Li, Z. Hou, W. Wang, J. Lin, *J. Solid State Chem.* **2009**, *182*, 1045.
[5] Y. Hikichi, T. Ota, K. Daimon, T. Hattori, *J. Am. Ceram. Soc.* **1998**, *81*, 2216.
[6] A. S. S. de Camargo, L. A. O. Nunes, D. R. Ardila, J. P. Andreeta, *Opt. Lett.* **2004**, *29*, 59.
[7] H. Zhu, H. Yang, D. Jin, Z. Wang, X. Gu, X. Yao, K. Yao, *J. Nanopart. Res.* **2008**, *10*, 1149.
[8] C. C. Wu, K. B. Chen, C. S. Lee, T. M. Chen, B. M. Cheng, *Chem. Mater.* **2007**, *19*, 3278.
[9] Y. Shimomura, T. Kurushima, R. Olivia, N. Kijima, *Jpn. J. Appl. Phys.* **2005**, *44*, 1356.
[10] F. Angiuli, F. Mezzadri, E. Cavalli, *J. Solid State Chem.* **2011**, *184*, 1843.
[11] G. Pan, H. Song, Q. Dai, R. Qin, X. Bai, B. Dong, L. Fan, F. Wang, *J. Appl. Phys.* **2008**, *104*, 084910.
[12] H. Yang, H. Lee, P. H. Holloway, *Nanotechnology* **2005**, *16*, 2794.
[13] H. Lai, B. Chen, W. Xu, X. Wang, Y. Yang, Q. Meng, *J. Alloys Compd.* **2005**, *395*, 181.
[14] Y. Z. Li, Y. H. Wang, Z. F. Wang, Z. Y. Zhang, *J. Lumin.* **2010**, *130*, 1225.
[15] N. S. Singh, R. S. Ningthoujam, S. D. Singh, B. Viswanadh, N. Manoj, R. K. Vatsa, *J. Lumin.* **2010**, *130*, 2452.
[16] D. Wang, Y. Wang, *Mater. Res. Bull.* **2007**, *42*, 2163.
[17] K. Riwotzki, H. Meyssamy, H. Schnablegger, A. Kornowski, M. Haase, *Angew. Chem. Int. Ed.* **2001**, *40*, 573.
[18] Z. Hou, L. Wang, H. Lian, R. Chai, C. Zhang, Z. Cheng, J. Lin, *J. Solid State Chem.* **2009**, *182*, 698.
[19] S. H. Jang, H. S. Tae, S. I. Chien, *IEEE Trans. Consum. Electron.* **2002**, *48*, 382.
[20] S. Kim, J. Seo, H. K. Jung, J. J. Kim, S. Y. Park, *Adv. Mater.* **2005**, *17*, 2077.
[21] J. Jiang, Y. Xu, W. Yang, R. Guan, Z. Liu, H. Zhen, Y. Cao, *Adv. Mater.* **2006**, *18*, 1769.
[22] J. M. Caruge, J. E. Halpert, V. Wood, V. Bulovic, M. G. Bawendi, *Nat. Photonics* **2008**, *2*, 247.
[23] A. A. Erchak, D. J. Ripin, S. Fan, P. Rakich, J. D. Joannopoulos, E. P. Ippen, G. S. Petrich, L. A. Kolodziejski, *Appl. Phys. Lett.* **2001**, *78*, 563.
[24] K. Y. Ko, K. N. Lee, Y. K. Lee, Y. R. Do, *J. Phys. Chem. C* **2008**, *112*, 7594.
[25] Y. K. Lee, J. R. Oh, Y. R. Do, *Appl. Phys. Lett.* **2007**, *91*, 041907.
[26] K. N. Lee, J. H. Moon, J. H. Oh, Y. R. Do, *J. Electrochem. Soc.* **2009**, *156*, J283.
[27] T. Yamasaki, K. Sumioka, T. Tsutsui, *Appl. Phys. Lett.* **2000**, *76*, 1243.
[28] Y. R. Do, Y. C. Kim, Y. W. Song, C. O. Cho, H. Jeon, Y. J. Lee, S. H. Kim, Y. H. Lee, *Adv. Mater.* **2003**, *15*, 1214.
[29] J. R. Oh, J. H. Moon, S. Yoon, C. R. Park, Y. R. Do, *J. Mater. Chem.* **2011**, *21*, 14167.
[30] W. S. Song, Y. S. Kim, H. Yang, *J. Electrochem. Soc.* **2011**, *158*, J137.
[31] S. Zhang, *IEEE Trans. Plasma Sci.* **2006**, *34*, 294.
[32] G. Buhler, C. Feldmann, *Appl. Phys. A* **2007**, *87*, 631.
[33] H. Althues, P. Simon, S. Kaskel, *J. Mater. Chem.* **2007**, *17*, 758.
[34] R. Chai, H. Lian, P. Yang, Y. Fan, Z. Hou, X. Kang, J. Lin, *J. Colloid Interface Sci.* **2009**, *336*, 46.
[35] H. D. Nguyen, S. I. Mho, I. H. Yeo, *J. Lumin.* **2009**, *129*, 1754.
[36] H. Lai, B. Chen, W. Xu, Y. Xie, X. Wang, W. Di, *Mater. Lett.* **2006**, *60*, 1341.